Third and Fourth Optical Transitions in Semiconducting Carbon Nanotubes

Paulo T. Araujo,[1] Stephen K. Doorn,[2] Svetlana Kilina,[3] Sergei Tretiak,[3] Erik Einarsson,[4] Shigeo Maruyama,[4]
Helio Chacham,[1] Marcos A. Pimenta,[1] and Ado Jorio[1]

[1]*Departamento de Física, Universidade Federal de Minas Gerais, Belo Horizonte, MG 30123-970, Brazil*
[2]*Chemistry Division, Los Alamos National Laboratory, Los Alamos, New Mexico 87545, USA*
[3]*Theoretical Division and Center for Nonlinear Studies, Los Alamos National Laboratory, Los Alamos, New Mexico 87545, USA*
[4]*Department of Mechanical Engineering, The University of Tokyo, Tokyo 113-8656, Japan*

We have studied the optical transition energies of single-wall carbon nanotubes over broad diameter
(0.7–2.3 nm) and energy (1.26–2.71 eV) ranges, using their radial breathing mode Raman spectra. We
establish the diameter and chiral angle dependence of the poorly studied third and fourth optical
transitions in semiconducting tubes. Comparative analysis between the higher lying transitions and the
first and second transitions show two different diameter scalings. Quantum mechanical calculations
explain the result showing strongly bound excitons in the first and second transitions and a delocalized
electron wave function in the third transition.

In carbon nanotubes [1], quantum confinement is responsible for 1D van Hove singularities in the electronic density of states and unusually strong many-body (electron-electron and electron-hole) interactions [2]. Current understanding of the photophysical properties of semiconducting carbon nanotubes [2–7] are based mostly on experimental results for the first (E_{11}^S) and second (E_{22}^S) optical transitions (*S* superscript stands for semiconducting, while *M* will be used for metallic tubes), based on a set of fewer than 40 SWNTs (characterized by their (n, m) indices [1]) in the diameter range from 0.7 to 1.3 nm [8–13]. Efforts have been made to extend these results to larger diameter tubes, and to establish the third (E_{33}^S) and fourth (E_{44}^S) transitions [14,15]. E_{33}^S and E_{44}^S are important for the optics of large diameter semiconducting single-wall carbon nanotubes (SWNTs), since for $d_t > 1.3$ nm, E_{22}^S is already in the infrared range [8–11].

Here we measure the optical properties of SWNTs over broad diameter (0.7–2.3 nm) and energy (1.26–2.71 eV) ranges. We probe over 200 different SWNT species, about 378 different optical transition energies, going up to the fourth optical transition of semiconducting SWNTs, thus establishing the (n, m) dependence of the poorly studied E_{33}^S and E_{44}^S transitions. Surprisingly, we find that E_{33}^S and E_{44}^S follow a different (blue-shifted) diameter scaling when compared with E_{11}^S and E_{22}^S. These results are supported by electronic structure calculations showing that E_{11}^S and E_{22}^S are described by bound exciton states, whereas the E_{33}^S transitions correspond to a delocalized exciton or to an unbound electron-hole pair.

The sample consists of as-grown vertically aligned SWNTs, synthesized by the chemical vapor deposition method from alcohol, on top of a quartz substrate. Transmission Electron Microscopy shows a rather homogeneous sample formed by isolated SWNTs and very small bundles [see inset of Fig. 1(d) and Refs. [16,17] for more details].

To determine the transition energies E_{ii} of each SWNT type separately, we use the resonance Raman scattering technique with a tunable laser excitation [9–11]. Two triple-monochromator Raman spectrometers, equipped with charge coupled device (CCD) detectors, were used in the back-scattering configuration to perform the measurements—a Dilor *XY* for experiments in the visible range and a SPEX in the near infrared range. We used a total of 95 different laser excitation energies (ArKr, Ti:Sapphire, and Dye lasers) from 1.26 eV to 2.71 eV. The light reaches the sample from the top, and the laser power density at the sample is maintained constant and low enough not to produce heating effects (1 mW focused with an 80× objective in the visible, and 25 mW focused with a 10 cm focal distance length in the infrared). A tungsten halogen lamp and 4-Acetamidophenol (tylenol) are used for calibration in the visible and infrared, respectively.

The 95 resonance Raman spectra were used to generate a two-dimensional plot giving the Raman intensity as a function of the laser excitation energy (E_{laser}) and radial breathing mode frequency (ω_{RBM}), shown in Fig. 1(a). A Raman peak appears at a given ω_{RBM} whenever E_{laser} reaches the optical transition energy (E_{ii}), i.e., when resonance is established for a given carbon nanotube in the sample [9–11].

Figure 1(b) presents the same data as in (a), with two differences: (i) normalized so that the highest peak in each spectrum has an intensity equal to unity. The maximum intensity for the E_{22}^S resonance profile of semiconducting nanotubes [reddish part in Fig. 1(a) online] are at least 1 order of magnitude higher (and sharper) than the maximum intensity for the resonance profile of the higher levels. In the normalized plot (b), the E_{22}^S, E_{11}^M, E_{33}^S, and E_{44}^S can be
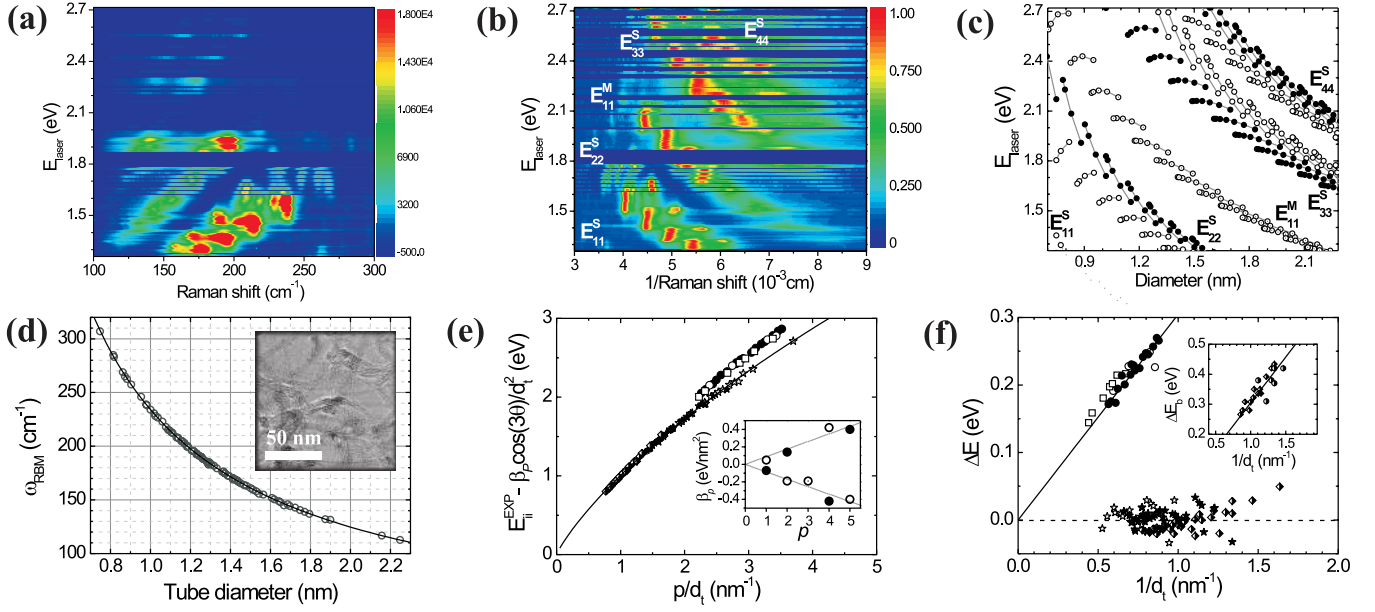
FIG. 1 (color online).   (a) 2D color map showing the SWNT RBM spectral evolution as a function of excitation laser energy. In (b), the intensity of each spectrum is normalized to the strongest peak, and we plot the inverse Raman shift. (c) The 378 optical transition energies (dots) of all SWNTs in the experimental range [20,21]. Grey lines are a guide to the eyes for SWNTs with $2n + m = $ const. Open, filled, and dotted circles stand for E_{ii} for semiconducting type 1 [$(2n + m)\mathrm{mod}3 = 1$], type 2 [$(2n + m)\mathrm{mod}3 = 2$], and metallic SWNTs [$(2n + m)\mathrm{mod}3 = 0$], respectively. (d) The ω_{RBM} versus tube diameter $d_t = 0.142\sqrt{3(n^2 + mn + m^2)}/\pi$. Circles are experimental data, and the solid line is given by $\omega_{\mathrm{RBM}} = 217.8/d_t + 15.7$. Inset: transmission electron microscopy image of the SWNT samples used in our experiment [17]. (e) Experimental optical transition energies as a function of p/d_t, after correcting for the chiral angle dependence ($E_{ii}^{\mathrm{EXP}} - \beta_p \cos 3\theta/d_t^2$). The chirality dependence corrected E_{11}^S (black and white diamonds from Ref. [8]), E_{22}^S (filled stars online), and E_{11}^M (open stars) are fitted with Eq. (1). Inset: the experimental β_p values for the lower (upper) E_{ii} branches are $-0.07(0.05)$, $-0.19(0.14)$, $-0.19(?)$, $-0.42(0.42)$, and $-0.4(0.4)$ for $p = 1, 2, 3, 4$, and 5, respectively. (f) Deviation (ΔE) of the ($E_{ii}^{\mathrm{EXP}} \cos 3\theta/d_t^2$) data from the fitting curve in (e), versus $1/d_t$. The solid line ($\Delta E = 0.305/d_t$) fits the ΔE_{33}^S (circles) and ΔE_{44}^S (squares). Inset: exciton binding energy ΔE_b obtained from Ref. [13] (circles) and Ref. [26] (diamonds), on top of the $\Delta E = 0.305/d_t$.

identified, while artificially elongated resonance profiles are related to SWNT families of constant $(2n + m)$ values [9–11]. (ii) plotted as a function of the inverse Raman frequency shift. The d_t is known to be related to $\omega^{-1}_{\mathrm{RBM}}$ [9–11,19], so that the resonance profile of each RBM Raman peak can be directly related to a given SWNT diameter.

The (n, m) assignment for each RBM observed in Fig. 1(b) can be made by directly comparing their resonance profiles with the so-called "Kataura plot" shown in Fig. 1(c). This plot shows the optical transition energies (dots) for every (n, m) SWNT as a function of tube diameter (see details in Refs. [9–11]). The transition energies are calculated with the nonorthogonal symmetry optimized extended tight-binding model, and are further upshifted to account for many-body corrections [19–21], being in excellent agreement with experimental results for E_{11}^S, E_{22}^S, and E_{11}^M from SWNT samples in the $0.7 < d_t < 1.3$ range [8–11].

Each of the 95 Raman spectra used to generate Fig. 2 was fit with a sum of Lorentzians (26 peaks on average), the number of Lorentzian peaks being consistent with the number of different (n, m) tubes expected to be in resonance for the considered excitation laser energy (ob-

tained from analysis of Fig. 1(c)—for details see [17]). From the fit, the ω_{RBM} is obtained with an experimental accuracy of ± 2 cm^{-1}. Using the relation $d_t = a_{\mathrm{C-C}}\sqrt{3(n^2 + mn + m^2)}/\pi$ [1], where $a_{\mathrm{C-C}} = 0.142$ nm is the carbon-carbon distance, ω_{RBM} is plotted against tube diameter in Fig. 1(d). Figure 1(d) shows the ω_{RBM} for 84 carbon nanotubes that can be well resolved experimentally. For the other tubes, the resonance profiles overlap with each other, and the radial breathing mode frequencies (as well as optical transition energies) cannot be clearly defined from the experimental profiles. The data in Fig. 1(d) can be fit within experimental accuracy by the simple expression $\omega_{\mathrm{RBM}} = A/d_t + B$, with $A = (217.8 \pm 0.3)$ cm^{-1} nm and $B = (15.7 \pm 0.3)$ cm^{-1} [17,22].

Next, we discuss the optical transition energies (E_{ii}) obtained from analysis of the intensity of the resonance profiles in Fig. 1(a) (for technical details see [9,17]). For a fixed SWNT chirality, the E_{ii} values are expected to exhibit a simple scaling behavior when plotted as a function of p/d_t, where $p = 1, 2, 3, 4, 5$, for $E_{11}^S, E_{22}^S, E_{11}^M, E_{33}^S, E_{44}^S$, respectively [7]. To a first approximation, considering the linear dispersion of the graphene and wave vector quantization, the optical transition energies in carbon nanotubes are given by $E_{ii} = \hbar v_F (4p/3d_t)$ [1], where v_F is the Fermi
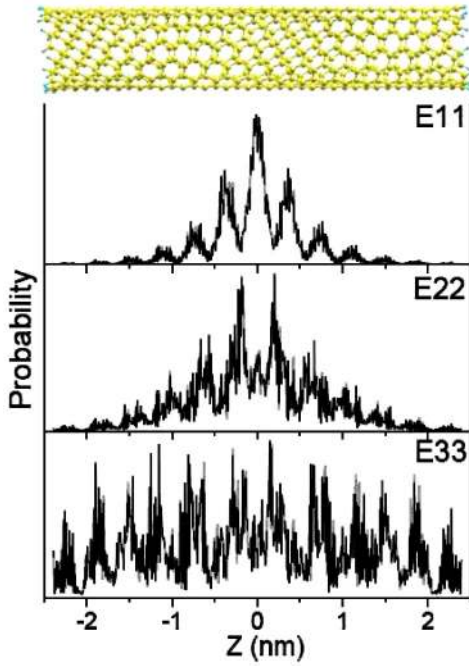
FIG. 2 (color online). Traces from top to bottom plot the electronic probability distribution for excited electrons on E_{11}^S, E_{22}^S, and E_{33}^S, respectively, along the (7,6) SWNT shown on top, considering the hole fixed in the middle.

velocity. The tube is metallic if p is a multiple of 3, and semiconducting otherwise [1]. The E_{ii} values also exhibit a small dependence on the chiral angle θ (ranging from 0 to 30°) [1]. The chirality correction is vanishing for armchair tubes ($\theta = 30°$) and is a maximum for zigzag tubes ($\theta = 0$), given approximately by $\beta_p \cos 3\theta / d_t^2$ [1]. All these trends can be seen in Fig. 1(c).

Figure 1(e) shows a plot of the transition energies E_{11}^S, E_{22}^S, E_{11}^M, E_{33}^S, E_{44}^S as a function of p/d_t, after correction for their chirality dependence obtained by subtracting $\beta_p \cos 3\theta / d_t^2$ from the experimentally obtained E_{ii} values (see inset for β_p values, $1 \leq p \leq 5$). Such a chirality correction is expected to collapse all E_{ii} values onto a single (p/d_t) dependent curve [7]. Note that the points do not scale linearly as p/d_t. As discussed by Kane and Mele [7], the nonlinear scaling is due to many-body effects and can be fit with a logarithmic correction [see Eq. (1) below] that comes from a full, nonperturbative renormalization group analysis of interacting electrons in a graphite layer [23]. However, the most interesting and indeed unexpected fact is that the E_{33}^S and E_{44}^S transitions do not follow the same scaling law as the E_{11}^S and E_{22}^S transitions, indicating that there is something fundamentally different between the first two lowest energy optical transitions and the subsequent transitions in semiconducting SWNTs.

To gain more insight into the different scaling laws for the E_{33}^S and E_{44}^S experimental data, consider Fig. 1(f). The chirality dependence corrected E_{11}^S, E_{22}^S, and E_{11}^M values plotted in Fig. 1(e) can be fit by [7,17,24]

$$E_{ii}(p, d_t) - \beta_p \cos 3\theta / d_t^2 = a\frac{p}{d_t}\left[1 + b\log\frac{c}{p/d_t}\right], \quad (1)$$

with $a = 1.049$ eV $\cdot$ nm, $b = 0.456$, and $c = 0.812$ nm^{-1}. This functional carries both the linear dependence of E_{ii} on p/d_t, expected from quantum confinement of the 2D electronic structure of graphene, and the many-body logarithmic corrections [7]. Figure 1(f) shows the deviation (ΔE) of the chirality dependence corrected ($E^{\mathrm{EXP}}_{ii} - \beta_p \cos 3\theta / d_t^2$) values from the right side of Eq. (1). The deviations ΔE_{33}^S and ΔE_{44}^S from the zero line in Fig. 1(f) show a clear $1/d_t$ dependence, and can be successfully fit by a single expression $\Delta E = \gamma/d_t$, with $\gamma = (0.305 \pm 0.004)$ eV $\cdot$ nm [25]. This blueshift for the higher lying transitions suggests E_{33}^S and E_{44}^S transitions exhibit weaker (or even null) exciton binding energy when compared to the lower lying levels. The inset of Fig. 1(f) plots the reported data for the measured exciton binding energies ΔE_b in SWNTs (symbols) [12,13,26], together with our linear dependence $\Delta E = 0.305/d_t$ (line), showing a surprising agreement between the two sets of experiments. This result suggests removing the exciton binding energy, i.e., the E_{33}^S and E_{44}^S transitions would be related to weakly bound (or unbound) electron-hole states.

To interpret the experimental results, we use the Collective Electronic Oscillator (CEO) technique to determine the excitonic delocalization of nanotubes. This quantum chemical methodology was successfully used in the past for a number of organic conjugated molecules [27,28] and recently for carbon nanotubes [29] for analysis of excitonic delocalization and vibronic effects. We have considered finite size chiral tubes (9,4) (type 1) and (7,6) (type 2) with one repeat unit in length. Each system considered has about 500 carbon atoms and a 5 nm length, sufficiently long to minimize edge effects. The tube ends were capped with hydrogens to saturate all broken bonds. For both tubes, we calculated all excited states within the 0–4.3 eV spectral window (which corresponds to about 600 states in each system) and identified E_{11}^S, E_{22}^S, and E_{33}^S excitonic states based on the oscillator strength.

To analyze the excitonic delocalization, we used a real space analysis based on the transition density matrices developed previously [27,28]. For the E_{11}^S, E_{22}^S, and E_{33}^S excitations, Fig. 2 plots the distributions of the photoexcited electron wave functions when the hole has been fixed in the middle of the (7,6) tube, averaged over the radial distribution. As illustrated by Fig. 2, the E_{11}^S and E_{22}^S states correspond to tightly bound excitons with a maximum electron-hole separation not exceeding 4 nm. This agrees well with previous theoretical studies of excitonic effects in SWNTs [2,4–6]. The E_{33}^S state, however, displays a very different behavior. It is nearly uniformly delocalized over the entire tube, confined by the tube's ends. This corresponds to either an unbound or a weakly bound excitonic state. Very similar results are obtained for the (9,4) tube. Furthermore, note that while the calculations have been

made for a $d_t = 0.88$ nm SWNTs, the same result should hold for wider diameters since the exciton binding energy is predicted to decrease with increasing diameter, scaling as $1/d_t$ [2–7].

We point out that our computational results contradict previous theoretical studies based on a first principles approach utilizing the Bethe-Salpeter equation and the *GW* approximation [2,17]. The latter imposes periodic boundary conditions on a perfect tube, where the wave vector k allows for efficient separation of ''pure'' excitonic bands. The E_{33}^S and E_{44}^S emerge from these calculations as tightly bound excitons, with the binding energy comparable or exceeding that of the first and second levels [2]. Barring differences between the theoretical methods, theory provides another scenario which could explain the fact that the excitonic nature of the higher transitions is observed to be different from that of the lower lying transitions: at the bottom of the E_{33}^S zone, there is a large density of states from E_{11}^S and E_{22}^S corresponding to the delocalized and unbound states. Consequently, the mixing of all these states and non-Condon effects might become important. This effect should be enhanced for E_{33}^S and E_{44}^S transitions as compared to E_{22}^S, since our calculations estimate less than 0.001 eV separation in the density of states at the E_{33}^S transition, attributed to other molecular states, compared to about an 0.02 eV separation at the E_{22}^S transition. Several recently published studies support this conjecture by pointing to the signature of this phenomenon, even at E_{22}^S level (e.g., see [30]).

In summary, we have studied the resonance Raman profile of more than 200 single-wall carbon nanotubes over a broad range of diameters and transition energies. We establish the diameter and chiral angle dependence for the radial breathing mode and for E_{ii} transitions up to E_{44}^S over this broad range. The E_{33}^S and E_{44}^S transitions always show anomalous scaling, being blue-shifted with respect to the E_{11}^S and E_{22}^S scaling law. The observed anomalies are explained by a large delocalization for the electrons in the higher lying levels, in contrast with the tightly bound excitons on the first and second transitions, as shown by quantum chemical calculations.

[1] R. Saito, G. Dresselhaus, and M. S. Dresselhaus, *Physical Properties of Carbon Nanotubes* (Imperial College Press, London, 1998).

[2] C. D. Spataru, S. Ismail-Beigi, L. X. Benedict, and S. G. Louie, Phys. Rev. Lett. **92**, 077402 (2004).

[3] C. L. Kane and E. J. Mele, Phys. Rev. Lett. **90**, 207401 (2003).

[4] E. Chang, G. Bussi, A. Ruini, and E. Molinari, Phys. Rev. Lett. **92**, 196401 (2004).

[5] V. Perebeinos, J. Tersoff, and Ph. Avouris, Phys. Rev. Lett. **92**, 257402 (2004).

[6] H. Zhao and S. Mazumdar, Phys. Rev. Lett. **93**, 157402 (2004).

[7] C. L. Kane and E. J. Mele, Phys. Rev. Lett. **93**, 197402 (2004).

[8] S. M. Bachilo *et al.*, Science **298**, 2361 (2002).

[9] C. Fantini *et al.*, Phys. Rev. Lett. **93**, 147406 (2004).

[10] H. Telg *et al.*, Phys. Rev. Lett. **93**, 177401 (2004).

[11] S. K. Doorn *et al.*, Appl. Phys. A **78**, 1147 (2004).

[12] F. Wang, G. Dukovic, L. E. Brus, and T. F. Heinz, Science **308**, 838 (2005).

[13] J. Maultzsch *et al.*, Phys. Rev. B **72**, 241402 (2005).

[14] Y. Matthew *et al.*, Science **312**, 554 (2006).

[15] M. Paillet *et al.*, Phys. Rev. Lett. **96**, 257401 (2006).

[16] Y. Murakami *et al.*, Carbon **43**, 2664 (2005).

[17] See EPAPS Document No. E-PRLTAO-98-007703 for larger version of Fig. 1(d), for E_{ii}, and ω_{RBM} obtained in this work. For more information on EPAPS, see http://www.aip.org/pubservs/epaps.html.

[18] J. C. Meyer *et al.*, Phys. Rev. Lett. **95**, 217401 (2005).

[19] V. N. Popov and L. Henrard, Phys. Rev. B **70**, 115407 (2004).

[20] Ge. G. Samsonidze *et al.*, Appl. Phys. Lett. **85**, 5703 (2004).

[21] A. Jorio *et al.*, Phys. Rev. B **71**, 075401 (2005).

[22] This result is in excellent agreement with the results in the recent literature applying to smaller diameter tubes ($d_t <$ 1.3 nm) [8–11]. A different d_t vs ω_{RBM} relation was proposed by Meyer *et al.* [18] based on measurements on larger diameter tubes. The difference is rather small, and it does not lead to a different (n, m) assignment. We also tried to use the relation by Meyer *et al.* and it does not represent a better fit to our data.

[23] J. Gonzalez, Phys. Rev. B **59**, R2474 (1999).

[24] The E_{22}^S values obtained here agree with the values obtained from isolated SWNT samples in solution [8–11]. We also tried to fit our data with a polynomial expansion on (p/d_t) and $(1/d_t)$. For a consistent fit, polynomials up to 5th order had to be used, with coefficients alternating sign, consistent with the logarithmic expansion in a power series. Two different curves, one for E_{11}^S and E_{22}^S, and another for E_{33}^S and E_{44}^S were always necessary.

[25] Figure 1(f) can be plotted as a function of (p/d_t), giving a linear dependence going to zero as well, but with slopes γ/p.

[26] G. Dukovic *et al.*, Nano Lett. **5**, 2314 (2005).

[27] S. Tretiak and S. Mukamel, Chem. Rev. **102**, 3171 (2002).

[28] S. Tretiak, A. Saxena, R. L. Martin, and A. R. Bishop, Phys. Rev. Lett. **89**, 097402 (2002).

[29] A. Gambetta *et al.*, Nature Phys. **2**, 515 (2006).

[30] C. Manzoni *et al.*, Phys. Rev. Lett. **94**, 207401 (2005).